JTTEE5 16:898–904
DOI: 10.1007/s11666-007-9108-6
1059-9630/$19.00 © ASM International

Solution Precursor Plasma Spray of Nickel-Yittia Stabilized Zirconia Anodes for Solid Oxide Fuel Cell Application

Y. Wang and T.W. Coyle

(Submitted March 12, 2007; in revised form July 15, 2007)

In conventional plasma spray of SOFC components, the large NiO and YSZ particles used, about 50-150 microns for high porosity coating, reduce the density of three-phase sites for electrode reaction. In this article, the SPPS process was used to synthesize and deposit Ni-YSZ anodes. The results show that several process parameters have significant effects on the microstructure and phase composition of the deposited material. The deposits were composed of tower-like, irregularly shaped agglomerates and smooth surface deposits. The sizes of the agglomerates increase with the decrease of the plasma-torch power and most are not completely molten during the impact. After heat treatment to reduce the NiO present in the as deposited coatings, the coatings were found to contain spherical YSZ particles about 0.5 μm in diameter distributed in a continuous Ni matrix, which is verified by both SEM observation and electrical resistance measurement. The coatings have 30-50% porosity.

Keywords microstructure, nickel-yittria stabilized zirconia (Ni-YSZ) anode, porosity, solid oxide fuel cell (SOFC), solution precursor plasma spray (SPPS)

1. Introduction

Since single-phase oxides for anode applications have not yet been successfully developed, Ni-Y_2O_3 stabilized ZrO_2 (Ni-YSZ) composites have been used for the anode material for solid-oxide fuel cells (SOFCs) with YSZ as the electrolyte. High-quality electrodes require the porosity to meet the following conditions: (i) 30-40 vol%; (ii) a homogenous pore size and pore distribution; and (iii) a large ratio of solid particle size to pore size, which will increase the continuity of pores to facilitate mass transport (Ref 1). In addition to the requirements for the pores, the desired microstructure for Ni and YSZ phases in the porous coating is: (i) 30-50 vol% Ni phase; (ii) homogenous sizes and distributions of the two phases; and (iii) a large ratio of YSZ particle diameter to Ni particle diameter to ensure high continuity of Ni phase. Although Ni-YSZ anodes deposited by conventional plasma spray are more successful than other SOFC components (Ref 2), the large NiO and YSZ particles used for the spray process, 50-150 microns for high-porosity coating deposition, reduce the three-phase sites for electrode reaction. In addition, NiO and YSZ powders for conventional plasma spray cannot be homogenously mixed due to the large density difference of the two powders, resulting in inhomogeneous distribution of the two phases in the fabricated coatings.

The solution precursor plasma spray (SPPS) process, in which a solution precursor of the desired resultant material is fed into a plasma jet by atomizing gas or high pressure, was developed in 1990s (Ref 3). The microstructure of the coatings produced by the SPPS process has ultra fine splats, and micrometer and nanometer porosity (Ref 4-7), which would provide more three-phase boundaries desirable for SOFC electrode applications. In addition, homogenously distributed Ni and YSZ phases in the fabricated coatings are expected, due to the homogeneity of the solution precursor. Furthermore, a microstructure with YSZ particles homogenously distributed in a continuous Ni matrix, which is desirable for SOFC anode application, could possibly be produced by the SPPS process due to the much lower melting point of Ni or NiO than that of YSZ. In summary, the SPPS process has the potential to deposit a highly efficient Ni-YSZ anode. However, there have been only a few published reports describing the use of direct current arc SPPS (DC-SPPS) to produce anodes (Ref 8). In this project, DC-SPPS was used to deposit Ni-YSZ anode material for SOFC application. The process parameter effects on the fabricated coatings were investigated; the microstructure and phase composition of the as-deposited and reduced coatings were characterized. In addition, the electrical resistance of the reduced coating was measured.

This article is an invited paper selected from presentations at the 2007 International Thermal Spray Conference and has been expanded from the original presentation. It is simultaneously published in *Global Coating Solutions, Proceedings of the 2007 International Thermal Spray Conference*, Beijing, China, May 14-16, 2007, Basil R. Marple, Margaret M. Hyland, Yuk-Chiu Lau, Chang-Jiu Li, Rogerio S. Lima, and Ghislain Montavon, Ed., ASM International, Materials Park, OH, 2007.

Y. Wang and **T.W. Coyle**, Centre for Advanced Coating Technologies, University of Toronto, Toronto, ON, Canada. Contact e-mail: yl.wang@utoronto.ca.

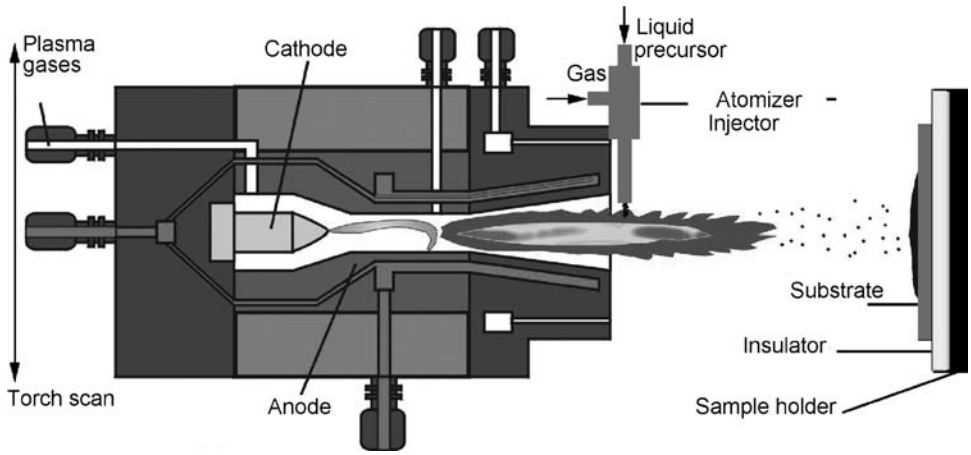

Fig. 1 DC-SPPS setup

2. Experimental Procedure

2.1 DC-SPPS Setup

The DC-SPPS setup consists of a solution precursor feeder system, a solution atomizer-injector (nozzle), an atmospheric plasma spray system, and a sample holder (Fig. 1). The solution precursor feeder system delivers measured quantities of the solution precursor to the atomizer-injector fixed on the front of the plasma torch, which produces atomized droplets of the precursor and injects them into the high-temperature plasma jet. A Miller SG-100 torch (Miller Thermal, Appleton, WI, USA) mounted on a robot was used. As the droplets enter the plasma jet, heat and momentum transfer from the plasma into the droplets leads to the evaporation of the solvent, condensation of the precursor, and plasma chemical reactions, resulting in the formation of a coherent deposit. Multiple passes of the torch were performed to build-up coatings.

2.2 Solution Precursor and Substrates

The solution precursor was made by adding distilled water to the mixture of $ZrOCl_2.8H_2O$, $Y(NO_3)_3.6H_2O$ and $Ni(NO_3)_3.6H_2O$. The amounts of the three nitrates were calculated to yield a cermet consisting of 60 vol% of 8 mol% Y_2O_3 partially stabilized ZrO_2 and 40 vol% Ni. Yttria partially stabilized zirconia discs with a nominal diameter of 2 cm were used as substrates, and thermally insulated from the steel sample holders.

2.3 Coating Characterization

The as-deposited, sintered, and reduced coatings were analyzed by scanning electron microscope (SEM) with energy dispersive x-ray analysis (EDX) (Model S-4500, Hitachi, Ltd., Japan) and x-ray diffraction (XRD) (Model CN2651A1, Rigaku Co., Japan). The porosity of the fabricated coatings was estimated by analyzing the SEM images of the sintered and reduced coating's polished cross sections using image analysis software (Clemex Vision PE 3.5, Longueuil, Quebec, Canada). The electrical resistances of the sintered and reduced coating were measured with a multimeter (HP Model 3435A, Hewlett-Packard Company, Loveland, Colorado, USA) at the temperature range from 20 to 800 °C in the gas mixture of 5% hydrogen and nitrogen.

3. Experiment Results

The range of processing parameters for which a NiO-YSZ composite can be generated was identified according to the plasma torch power capacity, the solubility of the metal salts, and so on. For the coatings deposited within the experimentally accessible parameter region, the phase composition and microstructure are dependent on several processing parameters. The power input to the plasma torch can be used as an example to describe the structure-processing parameter relations. In the following sections, the microstructures and phase composition of coatings deposited at low power (low power coating) and high power (high power coating) are characterized and compared. In addition, the electrical resistance versus temperature of a high power coating was measured and analyzed. Argon and hydrogen were used as plasma primary and secondary gases, respectively. The main processing parameters for high power coatings were: Ar flow rate 62SLM, H_2 flow rate 3SLM, arc voltage 55 V; arc current 630 A; standoff distance 7 cm; and solution flow rate 11 mL/min. This solution flow rate would ideally yield 1.23 g Ni-YSZ/min. For low power coatings, the H_2 flow rate was 1SLM, and the arc voltage and current were 45 V and 550 A, respectively; all other parameters are the same as those of high power coatings.

3.1 As Deposited Coatings

The microstructure of the surface and cross sections was characterized by SEM and EDX. The phase composition was analyzed by XRD.

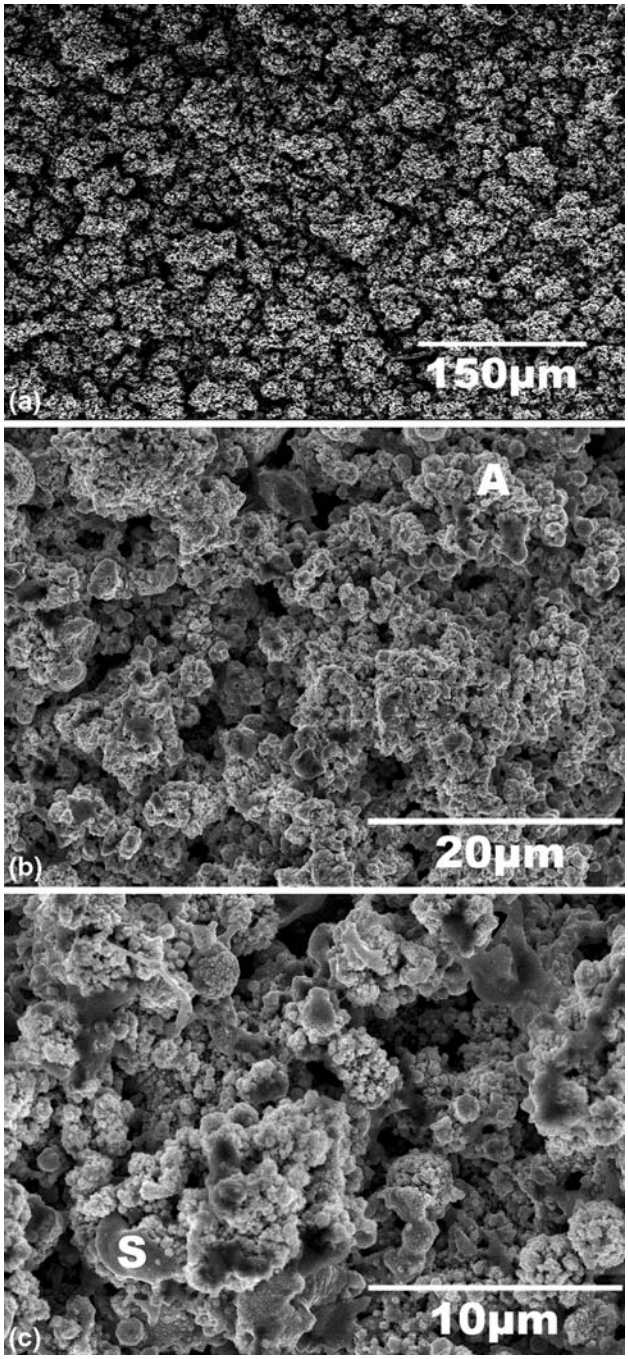

Fig. 2 SEM images of surface of as-deposited high power coatings, (a) surface of high power coating at low magnification; (b) and (c) surfaces of high power coatings at high magnifications

Figure 2(a) is a low magnification image of the surface of an as-deposited high power coating, showing that the coating's surfaces are rough but uniform. At high magnification as shown in Fig. 2(b) and (c), it can be seen that the high power coating is composed of agglomerates of small particles (A) and thin, smooth surface deposits (S). The agglomerates form irregular tower like shapes. The surfaces of the agglomerates are not smooth; there are tiny particles sticking on the surfaces as shown in Fig. 2(c). The smooth surface deposits are much smaller than the agglomerates in volume. EDX shows that the smooth surface deposits have the average element composition of the coatings. From the additional observations of coatings fabricated at different power levels, the relative amount of the smooth surface deposits was found to increase with increased power. Figure 3(a) is a surface image of a low power coating, showing that the coating was built up from agglomerates. The agglomerates stick together firmly and the surfaces of the agglomerates are not smooth. As in the high power coating, some of the agglomerates have tower-like shapes. The tower-like and irregularly shaped agglomerates in low power coatings are larger than those of high power coatings. The smooth surface deposits found in high power coatings were not observed in low power coatings. In addition, the agglomerates in both high and low power coatings were not deformed during impact on the substrate, indicating that the agglomerates were at most partially molten.

In order to investigate the coatings' microstructure further and the bond strength between the coatings' building elements, i.e., the agglomerates and smooth surface deposits, the as deposited coatings were fractured; the fractured cross sections were gold coated and observed by SEM. Figure 3(b) and (c) are SEM images of fractured cross sections of as deposited coatings at low magnification, which show that the coatings are very porous and that the pore size and pore distributions are homogenous. By comparison of the two pictures, it is clear that the pores and solid parts between the pores in the high power coating (Fig. 3b) are much smaller than those in the low power coating (Fig.3c). In both high and low power coatings almost all of the fractured cross section consists of planar features. Only a few concave or protruding features generated by pullout of agglomerates of small particles appear in the images. On the cross sections, about 10% of the fractured regions have the morphology of the B area in Fig. 4(a); the remaining regions have the morphology of the T area in the same figure. In the B area, the agglomerate of small particles remains almost intact; only a few fractured spots can be seen on the surface of the agglomerate, which means the B area is the preexisting surface of the agglomerate. In the T area, the agglomerate was cut by the fracture path; the small particles forming the agglomerate and holes inside the agglomerate are exposed after fracture, which is also shown by the area marked P in Fig. 4(b). Thus it appears that the fracture path over ~90% of the fractured area is through the agglomerates, meaning the bonds between agglomerates are strong enough to resist fracture.

The as-deposited high- and low-power coatings were analyzed by XRD to obtain the phase composition. The XRD of the low power coating in Fig. 5 indicates that the phases are NiO and 8YSZ. The high power coating has a similar XRD pattern, but all the peaks are much thinner, suggesting that the grain sizes of both phases in the high power coating are larger than those in the low power coating.

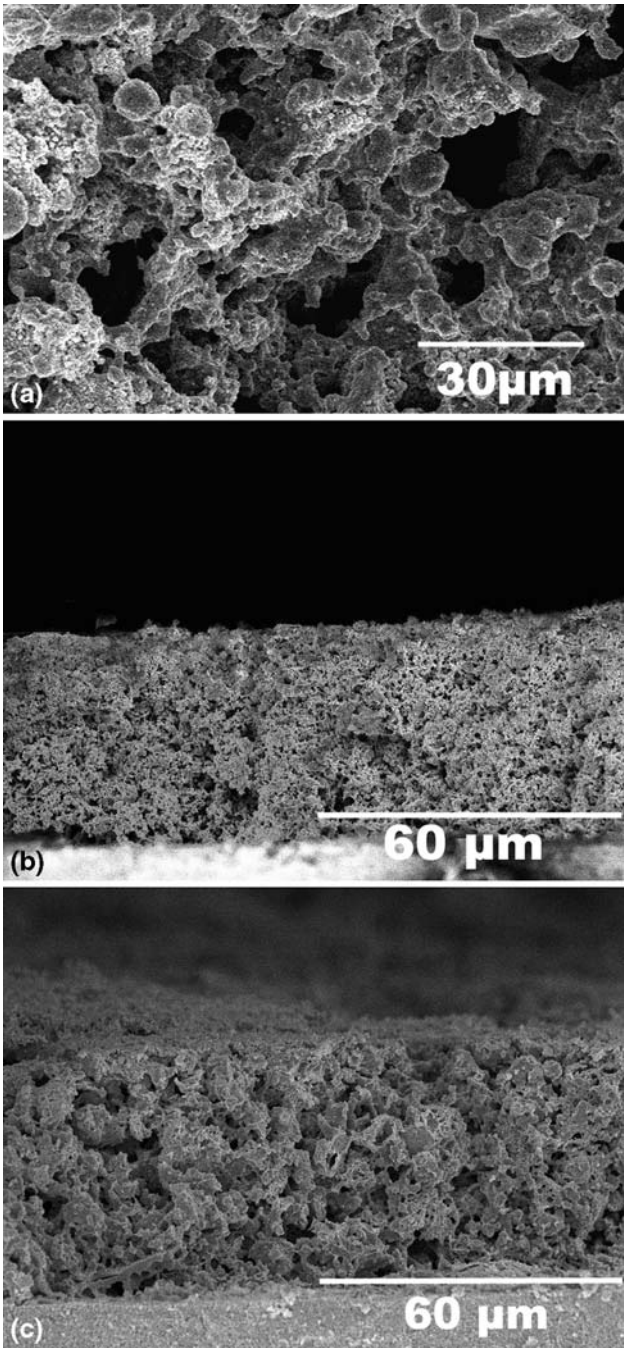

Fig. 3 SEM images of as-deposited coatings, (a) surface of low power coating; (b) fractured cross section of high power coating; (c) fractured cross section of low power coating

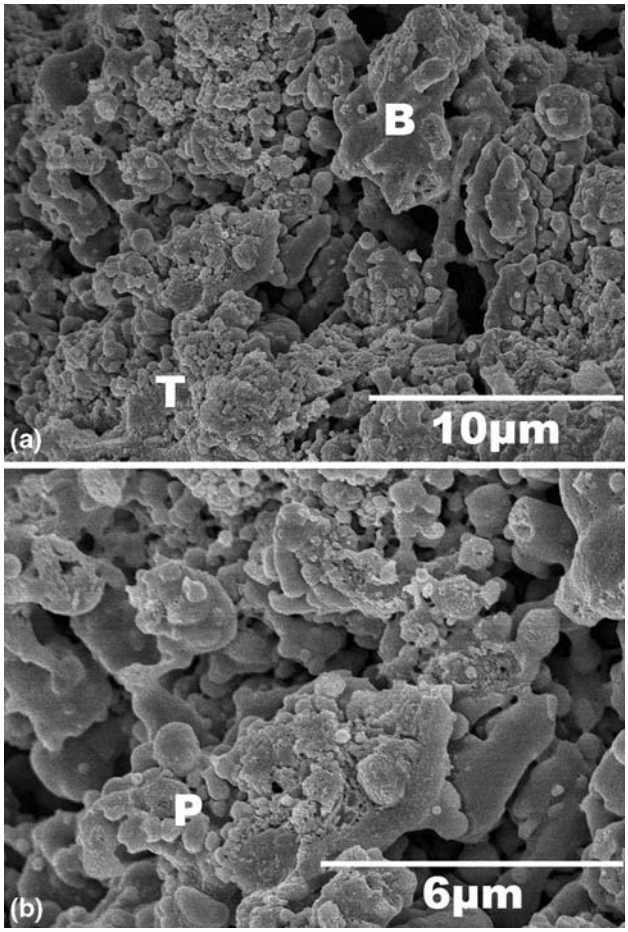

Fig. 4 SEM images of fractured cross sections of as-deposited high power coatings, (a) the fracture surface consists of preexisting agglomerate surfaces (B) and broken agglomerates (T); (b) the interior of a broken agglomerate is exposed (P), revealing the small spherical particles inside the agglomerate

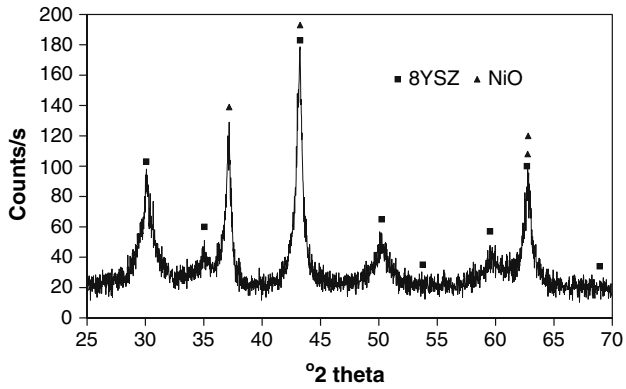

Fig. 5 XRD of as-deposited coating

In summary, the as-deposited coating consists of agglomerates with irregular tower-like shapes and smooth surface deposits. The smooth surface deposits are much smaller than the agglomerates in volume. The fraction of smooth surface deposits in the coatings increases with increase of the power. No smooth surface deposits were observed in the low power coating. The sizes of the pores and the agglomerates in the low power coating are larger than those in the high power coating. The agglomerates were strong enough to maintain their shapes during impact onto the substrate. Almost all the fracture path passes though the agglomerates. The phases present in the as deposited coatings are NiO and 8YSZ.

3.2 Sintered and Reduced Coatings

The synthesized coatings were sintered at 1250 °C for 5 h in air and reduced in a hydrogen atmosphere at 1000 °C to examine the stability of the microstructure and phase composition. The results from SEM, EDX, and XRD analysis are presented in the following:

As shown in Fig. 6, the sintered and reduced coating consists of an 8YSZ and Ni composite, indicating that NiO was successfully reduced to Ni. However, all the peaks are thinner than those in the XRDs of as-deposited coatings, which suggests that all the grains of 8YSZ and Ni grew during sintering and reduction.

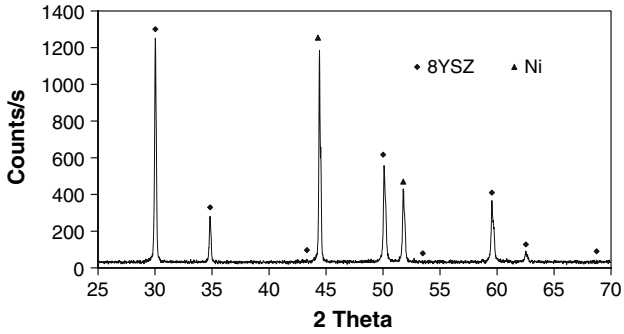

Fig. 6 XRD of sintered and reduced coating

After sintering and reduction, the tiny particles attached to the surfaces of the agglomerates in the as-deposited coatings disappear as shown in Fig. 7(a) and (c); the surfaces of the agglomerates become smooth. The sizes for most of the agglomerates in the high power coating are about 5 μm, while those in the low power coating are about 10 μm as demonstrated by Fig. 7(a) and (b). The tower-like agglomerates form multiple layers, as-marked by L in Fig. 7(a) and (b). As shown in Fig. 7(c), the agglomerates consist of small spherical particles approximately 0.5 μm in diameter. From the observations of coatings deposited at different powers, it is found that the small particles are always about 0.5 μm. There are smooth sheet-like regions in the images of the high power coating, such as, the regions marked by S in Fig. 7(c); EDX results indicate that the material here has the average composition of the coating. However, these regions were never found in the images of the low power sintered and reduced coating. It is reasonable to believe

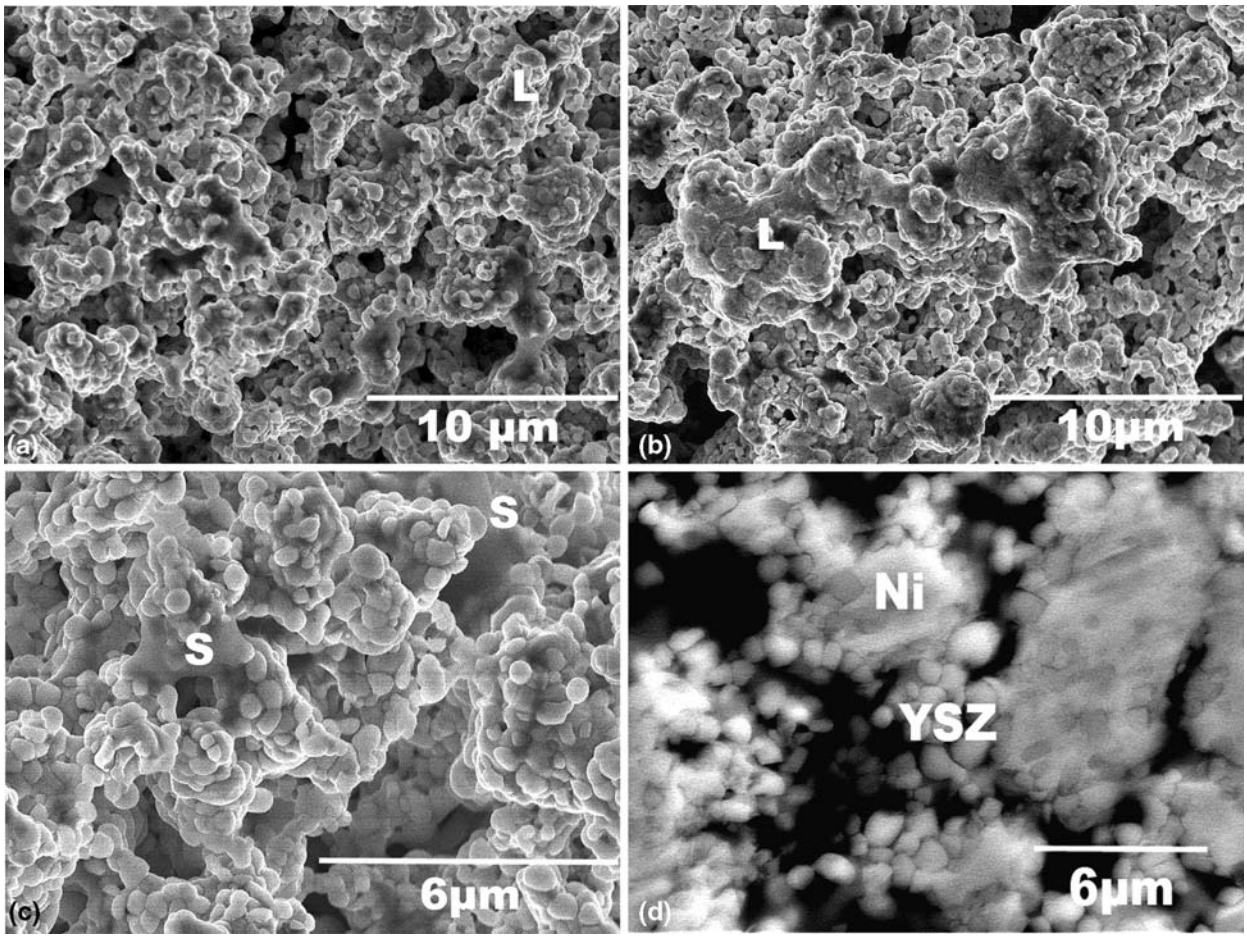

Fig. 7 SEM images of high power coatings, (a-c) surfaces of sintered and reduced coatings; (d) polished surface of sintered and reduced coating

that the regions are the smooth surface deposits found in the as deposited high power coating. As shown in the polished surface image of the sintered and reduced coating Fig. 7(d), two phases can be identified, one of which forms a continuous matrix and the other is made up of small round particles with a diameter of 0.5 μm held together by the continuous matrix phase. EDX indicates that the continuous matrix phase is Ni and the small spherical particles are YSZ. Therefore, we can conclude that the Ni-YSZ coatings are made of agglomerates of 0.5 μm YSZ particles held together by continuous Ni matrix.

Figure 8(a) is an image of a gold-coated polished cross section of a sintered and reduced coating, showing that the porosity is homogenous and the solid part is well connected. It is found from the image that there are two kinds of pores in the coating, large pores located between the agglomerates and fine pores inside the agglomerates. The analysis of the SEM images of the sintered and reduced coating's polished cross sections using the image analysis software shows that coatings with porosity ranging from 30 to 50 area percent could be obtained. The SEM images of the gold-coated fracture cross section of sintered and reduced coatings Fig. 8(b) and (c) shows that the fractured cross sections are rough and porous. The solid parts of the coating are well connected. The fractured cross section consists of two kinds of regions. One is the intact surfaces of preexisting large pores as marked by I in Fig. 8(b). The other is the fracture surface created when the crack passes through an agglomerate as marked by F in the same figure. In the fractured regions broken particles can be found, as shown in Fig. 8(c), indicating strong bonding between particles.

In summary, the sintered and reduced coating consists of a Ni-8YSZ composite. The tower-like agglomerates are composed of several layers; the dimensions for most of the agglomerates of the high power coating are about 5 μm, while those for the low power coating are about 10 μm; they consist of about 0.5 μm spherical YSZ particles held together by a continuous Ni matrix; the bonds between the small particles are strong.

3.3 Electrical Resistance of Ni-YSZ Coating

In a Ni-YSZ anode, both the Ni and YSZ phases must form continuous networks. In that case the overall conductivity of the sample would be determined by the Ni phase, because the conductivity of metallic Ni is five orders of magnitude higher than that of YSZ. In order to determine if the Ni phase was continuous in the present coatings, the electrical resistance of the sintered and reduced coating was measured with the digital multimeter at the temperature range from 20 to 800 °C in a gas mixture of 5% H_2 and N_2.

The inverse of the electrical resistance, $1/R$, is plotted versus temperature, T, in Fig. 9, which shows that $1/R$ decreases with increasing temperature. The slope is larger from 20 °C to the Curie temperatue of Ni (about 354 °C) than above the Curie temperature. Nickel is a ferromagnetic metal (Ref 9), the electrical conductivity of which can be divided into two parts. Above Curie temperature, normal metallic conductivity proportional to the reciprocal of the absolute temperature is observed. Below the Curie temperature the conductivity is characteristic of ferromagnetism, and drops quickly with increasing temperature. The observed change in resistance with temperature confirms that a continuous network of Ni exists in the coating.

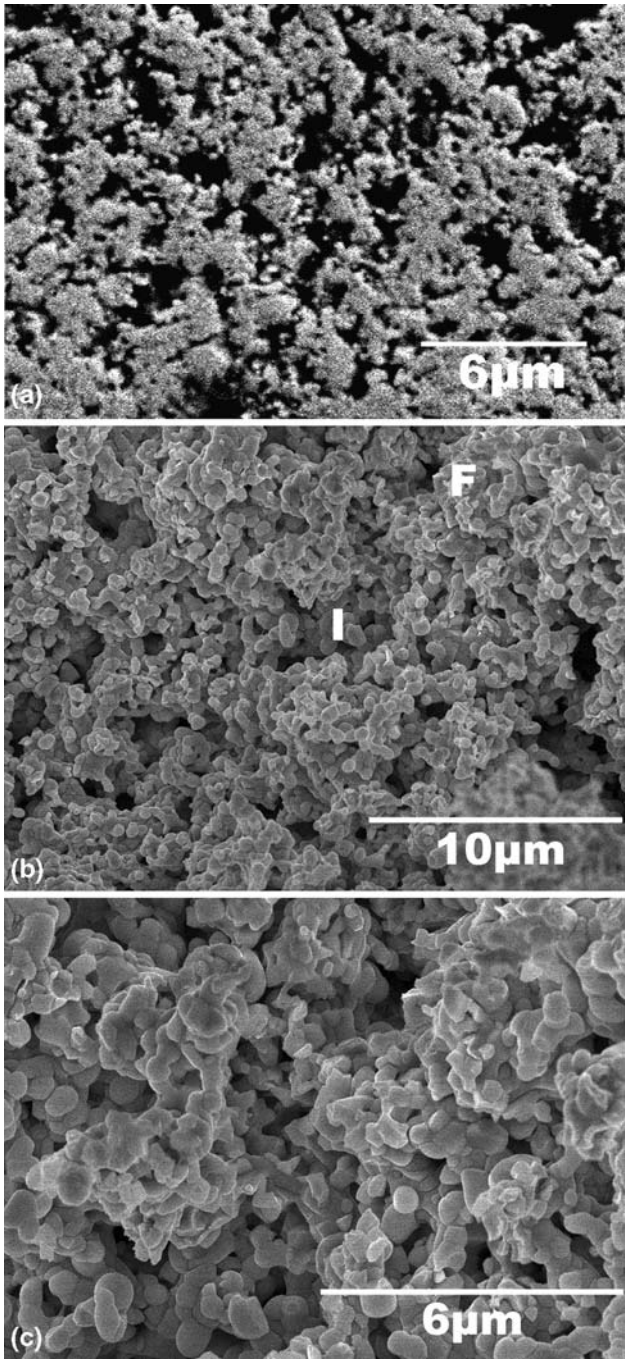

Fig. 8 SEM images of cross sections of sintered and reduced coatings. (a) Polished cross section; (b) and (c) Fractured cross sections

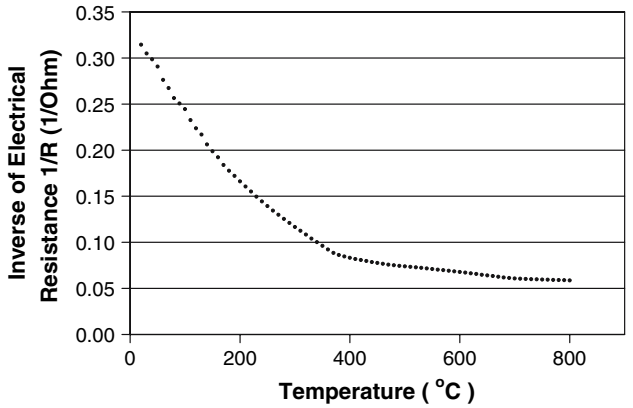

Fig. 9 Inverse of the electrical resistance of Ni-YSZ anode coating as a function of temperature in the gas mixture of 5% H_2 and N_2

4. Discussion

When a solution droplet enters the high temperature plasma jet, it will go through acceleration and break up, solvent evaporation, solute precipitation and decomposition, sintering and melting of the synthesized material and impact on the substrate. Although these processes have not been well understood, some insight into the deposition process can be gained from the nature of the deposits.

According to mass balance, one 20 μm diameter precursor droplet (Ref 7) should generate an agglomerate of YSZ and Ni composite with a diameter of about 4.6 μm if there is no breakup. The size of the agglomerates in the low power coating are about 10 μm as shown in Fig. 7(b), suggesting that agglomeration of smaller agglomerates must occur. The agglomeration of smaller agglomerates during flight process is consistent with the tower-like structure of the agglomerates as marked by L in Fig. 7(a) and (b).

A solution droplet suddenly exposed to high-speed plasma gases will be flattened and broken up by the aerodynamic pressure of the plasma gases. The faster the plasma gases, the smaller the size of the generated child droplets (Ref 10). The plasma gas velocity and temperature are higher when the plasma torch is operated at a high power (Ref 11, 12). The smaller droplets generated in the plasma jet of high power torch will form smaller agglomerates. Therefore, after agglomeration of these smaller agglomerates, the size of the final irregularly shaped tower-like structure will be smaller than in low power coating as illustrated in Fig. 7(a) and (b). A small fraction of the agglomerates, which pass through the high temperature core region of plasma jet were melted completely to form smooth surface deposits (S in Fig. 2c) upon impact onto the surface of coating.

5. Conclusions

Ni-YSZ SOFC anode coatings were successfully fabricated by a solution precursor plasma spray (SPPS) process. The coatings consist of both agglomerates of 0.5 μm spherical YSZ particles held together by a continuous Ni matrix and Ni-YSZ composite smooth surface deposits. The higher the plasma torch power, the smaller the size of the agglomerates. The amount of the smooth surface deposits is directly proportion to the power. There are two kinds of pores in the coatings, one of which is between the agglomerates and the other inside the agglomerates. Coatings with porosity of 30-50 area% were obtained in the experimentally accessible range of deposition conditions. Electrical resistance measurements and SEM observation indicate that a continuous network of nickel was formed in the coating.

Acknowledgment

This project was supported by the Strategic Skills Investment Program of the Ontario Ministry for Training, Colleges and Universities and by the Natural Science and Engineering Research Council of Canada. The authors would like to express gratitude to Dr. Pershin and Mr. Li for their kind help in the plasma spray experiments.

References

1. Z. Fan, A.P. Miodownik, and P. Tsakiropoulos, Microstructural Characterization of Two Phase Materials, *Mater. Sci. Technol.*, 1993, **9**, p 1094-1097
2. T. Yoshida, T. Okada, H. Hamatani, and H. Kumaoka, Integrated Fabrication Process for Solid Oxide Fuel Cells Using Novel Plasma Spraying, *Plasma Sources Sci. Technol.*, 1992, **1**, p 195-201
3. H. Wang, J. Williams, K.D. Vuong, C.Q. Shen, V. Wu, D.H. Lee, R.A. Condrate, and X.W. Wang, RF Plasma Fabrication of Nanoscaled Ceramic Oxides for Energy Devices, *Proceedings of 30th Intersociety Energy Conversion Engineering Conference*, D. Yogi Goswani, et al., Eds., 30 July-4 Aug. 1995 (Orlando, FL, USA) American Society of Mechanical Engineers, 1995, p 295-300
4. M. Gell, L. Xie, X. Ma, E.H. Jordan, and N.P. Padture, Highly Durable Thermal Barrier Coatings Made by the Solution Precursor Plasma Spray Process, *Surf. Coat. Technol.*, 2004, **177-178**, p 97-102
5. L. Xie, X. Ma, E.H. Jordan, N.P. Padture, D.T. Xiao, and M. Gell, Deposition of Thermal Barrier Coatings Using the Solution Precursor Plasma Spray Process, *J. Mat. Sci.*, 2004, **39**, p 1639-1646
6. L. Xie, X. Ma, E.H. Jordan, N.P. Padture, D.T. Xiao, and M. Gell, Deposition Mechanisms of Thermal Barrier Coatings in the Solution Precursor Plasma Spray Process, *Surf. Coat. Technol.*, 2004, **177-178**, p 103-107
7. Y. Wang and T. W. Coyle, Solution Precursor Plasma Spray (SPPS) of Porous La_{1-x} Sr_xMnO_3 (LSM) Perovskite Coatings for SOFC Cathode Application, Submitted to J. Fuel Cell Sci. Technol
8. X. Ma, J. Dai, H. Zhang, J. Roth, T.D. Xiao, and D.E. Reisner, Solid Oxide Fuel Cell Development by Using Novel Plasma Spray Techniques, *J. Fuel Cell Sci. Technol.*, 2005, **2**, p 190-196
9. T. Kasuya, Electrical Resistance of Ferromagnetic Metals, *Prog. Theor. Phys.*, 1956, **16**(1), p 58-63
10. H.E. Wolfe and W.H. Andersen, Kinetics, Mechanism, and Resultant Droplet Sizes of the Aerodynamic Breakup of Liquid Drops, Aerojet-General Corporation Research and Engineering Division Report No. 0395-04 (18) SP, 1964
11. M.P. Planche, J.F. Coudert, and P. Fauchais, Velocity Measurements for Arc Jets Produced by a DC Plasma Spray Torch, *Plasma Chem. Plasma Process.*, 1998, **18**(2), p 263-283
12. S. Semenov and B. Cetegen, Spectroscopic Temperature Measurement in Direct Current Arc Plasma Jets Used in Thermal Spray Processing of Materials, *J. Therm. Spray. Technol.*, 2001, **10**(2), p 326-336